



Available online at www.sciencedirect.com



00 (2023) 1–18



A Linear Quadratic Integral Differential Game Approach for Attitude Control of an Experimental Platform of a Quadrotor

Hadi Nobahari, Ali BaniAsad, Reza Pordal, Alireza Sharifi

Department of Aerospace Engineering Sharif University of Technology Tehran, Iran

Abstract

In this study, a linear quadratic integral differential game approach is applied to regulate and track the attitude angle of an experimental setup of the quadrotor using two players. One produces commands for each channel of the quadrotor and another creates the worst disturbance by minimizing a quadratic criterion with integral action. For this purpose, first, the attitude dynamics of the platform are modeled and its parameter is identified based on the Nonlinear Least Squares Trust-Region Reflective Least Squares method. The performance of the proposed controller is evaluated for regulation and tracking problems. The ability of the controller is examined in the disturbance rejection. Moreover, the influence of uncertainty modeling is studied on the obtained results. Then, the performance of the proposed controller is compared with a classic PID, Linear Quadratic Regulator, and Linear Quadratic Integral Regulator. The result demonstrates the effectiveness of the Game Theory on the Linear Quadratic Regulator approach when the input disturbance occurs.

© 2011 Published by Elsevier Ltd.

Keywords:

Linear quadratic Gaussian controller, Differential game theory, Quadrotor, Continuous state-space model, three-degree-of-freedom experimental platform, Attitude Control Optimization, Robust disturbance rejection.

1. Introduction

The investigation, strategic operations, optical sensing, entertainment, and farming are all used by quadrotors in today's society [1]. Various subsystems of the quadrotor control system are responsible for the quadrotor's performance, including attitude, altitude, and position. Maintaining the desired attitude outputs is essential for quadrotor attitude control, particularly in the presence of sudden disturbances. This can be achieved by controlling the rotor rotational speeds[2]. Consequently, there is a growing body of research focusing on the development of automatic control strategies for quadrotors to effectively manage disturbances and maintain desired attitudes. The quadrotor attitude is controlled by a Proportional Integral Derivative (PID) controller in [3, 4]. During disturbances, however, this controller has not effectively achieved the control objectives. Model-based approaches to controller design are utilized to resolve this issue [5, 6]. Quadrotor attitude models and disturbances determine the direction of the best control commands using these controllers.

Email addresses: nobahari@sharif.edu (Hadi Nobahari), ali.baniasad@ae.sharif.edu (Ali BaniAsad), email address (Reza Pordal), alireza_sharifi@ae.sharif.edu (Alireza Sharifi)

The literature has proposed numerous models-based controllers to provide a faster control algorithm when dealing with modeling errors and reducing disturbances. An intelligent controller, a robust controller, a nonlinear controller, and an optimal controller are some of these types of controllers.

Various control approaches based on intelligent logic, such as machine learning [7], evolutionary computation [8], iterative learning [9], reinforcement learning [10], and fuzzy logic [11], have been extensively employed for quadrotor attitude regulation. Numerous nonlinear control techniques have been proposed to regulate orientation angles of quadrotors, including Synergetic Control [12], Sliding Mode Control (SMC) [13], and Feedback Linearization (FBL) [14]. Robust control methods such as H_∞ [15, 16] and μ -synthesis [17] have also been utilized to stabilize the attitudes of quadrotors under conditions of extreme uncertainty and worst-case scenarios. Quadrotors have also been controlled using optimal controllers, such as the Linear Quadratic Gaussian (LQG) [18] and the Linear Quadratic Regulator (LQR) [19]. Optimizing feedback gains is achieved by utilizing both regulation and control effort to minimize a quadratic criterion. The Linear Quadratic Regulator Differential Game (LQR-DG) is a robust and optimal control strategy that has been extensively utilized in controlling various nonlinear and complex systems, including quadrotors. This approach employs a linear system model to control its outputs while minimizing a cost function through minimaximization. The LQR-DG approach has been demonstrated to offer excellent regulation performance and control effort while being robust to external disturbances. For instance, it has been successfully applied to control a ship controller, showcasing its effectiveness and versatility in handling complex control problems [20, 21]. By means of an analytical pursuit-evasion process, the LQR-DG control approach generates precise and optimized control commands. This unique feature sets the LQR-DG controller apart from other conventional optimal control techniques and enables one player to track the most appropriate control command while the other creates disturbances.

In this paper, an LQIR method, called LQIR-DG controller is suggested to produce the optimal and robust control command, i.e. rotational velocity command using the game theory approach. Since the LQIR-DG controller is affected by an exact model of the plant, the quadrotor's experimental platform is modeled and its parameters are identified based on experimental data. For control purposes, its linear state-space form is extracted using linearization of the nonlinear UAV. Then, the LQIR-DG technique is applied in real-time to the experimental platform. The performance of the LQIR-DG method is evaluated in the presence of the disturbance and modeling error for regulation and tracking purposes. A comparison is also performed between the results of classical PID, LQR, and LQIR and the proposed approach in real-time mode. The results show the proposed control structure is effective in the control of the quadrotor platform.

The following sections of this research paper provide a comprehensive analysis of the proposed control approach. Section 2 defines detailed derivations of the dynamics model and quadrotor's experimental platform, respectively. Section 4 explicates the proposed LQIG-DG controller architecture. The effectiveness of the controller is assessed in section 5, which is followed by the conclusion in section 6.

2. Problem Formulation

The experimental quadrotor platform rotates freely with rotational velocity about its roll, pitch, and yaw axes, as shown in Figure 1. The Euler angles and their derivatives are measured using an Attitude Heading Reference System (AHRS), which is utilized in the structure of the LQIR-DG controller to stabilize the quadrotor platform. The graphical representation of the proposed controller structure is depicted in Figure 2.



Figure 1: 3DoF setup of the quadrotor.

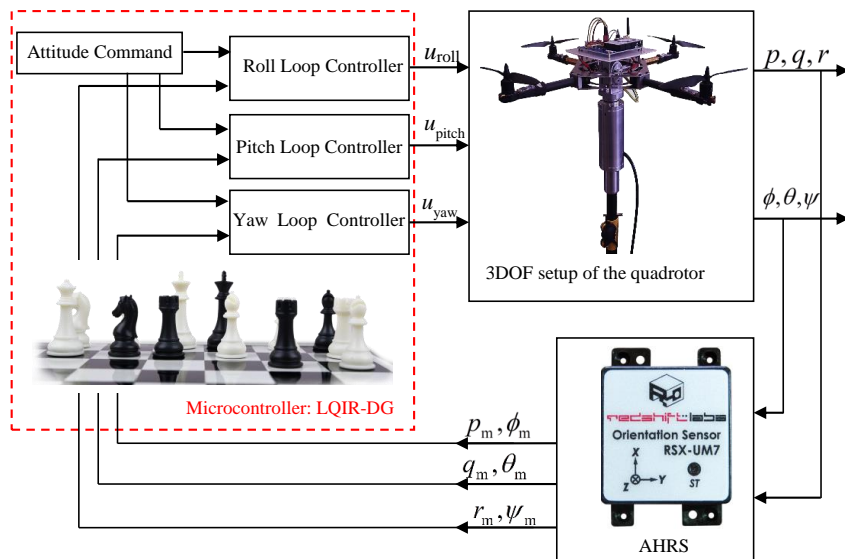


Figure 2: Structure of the LQIG-DG Controller Illustrated in a Block Diagram.

3. Dynamic Model of the Quadrotor Platform

In this section, first, a nonlinear model for the quadrotor platform is derived. Then, a state-space model and a linear model are developed for control purposes to be utilized in a controller strategy. Finally, a nonlinear identification method is applied to identify the parameters of the quadrotor.

3.1. Quadrotor Configuration

Figure 3 shows the quadrotor schematic. It depicts four rotors rotating around the z_B axis in the coordinate system of the body. The rotors have a rotational velocity of Ω_r . The quadrotor platform has 3 degrees of freedom,

including roll, pitch, and yaw motions, which are described by roll (ϕ), pitch (θ), and yaw (ψ) angles, respectively. The counterclockwise rotation of Rotors 1 and 3 generates a moment that counteracts the yawing moment, while the clockwise rotation of Rotors 2 and 4 produces a moment that also counteracts the yawing moment.

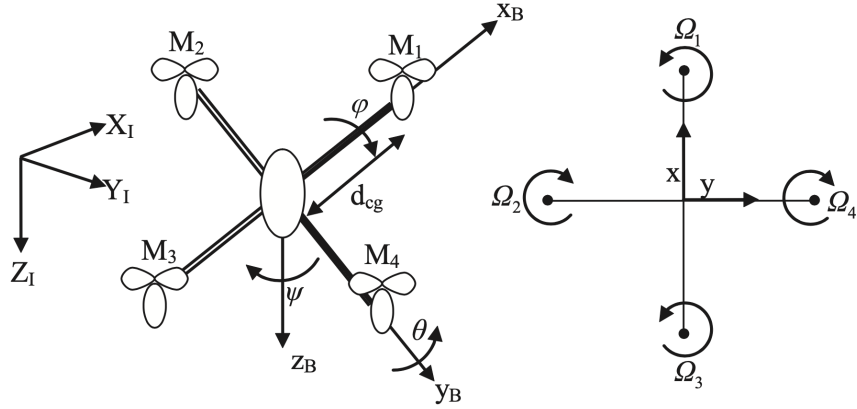


Figure 3: Quadrotor Configuration.

3.2. Dynamic Modeling of the Quadrotor Platform

Here, according to Newton-Euler, the dynamic model of the quadrotor platform is derived as follows [22, 23]:

$$\dot{p} = \frac{I_{yy} - I_{zz}}{I_{xx}} qr + q \frac{I_{rotor}}{I_{xx}} \Omega_r + \frac{u_{roll}}{I_{xx}} + \frac{d_{roll}}{I_{xx}} \quad (1)$$

$$\dot{q} = \frac{I_{zz} - I_{xx}}{I_{yy}} rp + p \frac{I_{rotor}}{I_{xx}} \Omega_r + \frac{u_{pitch}}{I_{yy}} + \frac{d_{pitch}}{I_{yy}} \quad (2)$$

$$\dot{r} = \frac{I_{xx} - I_{yy}}{I_{zz}} pq + \frac{u_{yaw}}{I_{zz}} + \frac{d_{yaw}}{I_{zz}} \quad (3)$$

The (p, q, r) represent the rotational variables, and d_{roll} , d_{pitch} , and d_{yaw} denote the disturbances produced in the x_B , y_B , and z_B axes, respectively. Additionally, I_{xx} , I_{yy} , and I_{zz} are the principal moments of inertia, and I_{rotor} is the rotor inertia about its axis. Euler angle rates are also determined from angular body rates as follows:

$$\begin{bmatrix} \dot{\phi} \\ \dot{\theta} \\ \dot{\psi} \end{bmatrix} = \begin{bmatrix} 1 & \sin(\phi) \tan(\theta) & \cos(\phi) \tan(\theta) \\ 0 & \cos(\phi) & -\sin(\phi) \\ 0 & \sin(\phi)/\cos(\theta) & \cos(\phi)/\cos(\theta) \end{bmatrix} \begin{bmatrix} p \\ q \\ r \end{bmatrix} \quad (4)$$

The residual rotor velocity, denoted by Ω_r , is calculated as follows:

$$\Omega_r = -\Omega_1 + \Omega_2 - \Omega_3 + \Omega_4 \quad (5)$$

3.3. Input of the Dynamic Model

The control inputs u_{roll} , u_{pitch} , and u_{yaw} are to the moments generated by the quadrotor's rotors along the roll, pitch, and yaw axes, respectively, defined as follows:

$$u_{roll} = b d_{cg} (\Omega_2^2 - \Omega_4^2) \quad (6)$$

$$u_{pitch} = b d_{cg} (\Omega_1^2 - \Omega_3^2) \quad (7)$$

$$u_{yaw} = d (\Omega_1^2 - \Omega_2^2 + \Omega_3^2 - \Omega_4^2) \quad (8)$$

where d_{cg} , d , and b represent the distance between the rotors and the gravity center, drag factor, and thrust factor, respectively. The rotational velocity commands are computed as follows:

$$\Omega_{c,1}^2 = \Omega_{\text{mean}}^2 + \frac{1}{2b d_{cg}} u_{\text{pitch}} + \frac{1}{4d} u_{\text{yaw}} \quad (9)$$

$$\Omega_{c,2}^2 = \Omega_{\text{mean}}^2 + \frac{1}{2b d_{cg}} u_{\text{roll}} - \frac{1}{4d} u_{\text{yaw}} \quad (10)$$

$$\Omega_{c,3}^2 = \Omega_{\text{mean}}^2 - \frac{1}{2b d_{cg}} u_{\text{pitch}} + \frac{1}{4d} u_{\text{yaw}} \quad (11)$$

$$\Omega_{c,4}^2 = \Omega_{\text{mean}}^2 - \frac{1}{2b d_{cg}} u_{\text{roll}} - \frac{1}{4d} u_{\text{yaw}} \quad (12)$$

In the above equation, Ω_{mean} is nominal rotational velocities of the rotors.

3.4. State-Space Formulation

Here, by defining $x_1 = p$, $x_2 = q$, $x_3 = r$, $x_4 = \phi$, $x_5 = \theta$, and $x_6 = \psi$, the formulation of the quadrotor platform is presented as follows:

$$\dot{x}_1 = \Gamma_1 x_2 x_3 + \Gamma_2 x_2 \Omega_r + \Gamma_3 u_{\text{roll}} + \Gamma_3 d_{\text{roll}} \quad (13)$$

$$\dot{x}_2 = \Gamma_4 x_1 x_3 - \Gamma_5 x_1 \Omega_r + \Gamma_6 u_{\text{pitch}} + \Gamma_6 d_{\text{pitch}} \quad (14)$$

$$\dot{x}_3 = \Gamma_7 x_1 x_2 + \Gamma_8 u_{\text{yaw}} + \Gamma_8 d_{\text{yaw}} \quad (15)$$

$$\dot{x}_4 = x_1 + (x_2 \sin(x_4) + x_3 \cos(x_4)) \tan(x_5) \quad (16)$$

$$\dot{x}_5 = x_2 \cos(x_4) - x_3 \sin(x_4) \quad (17)$$

$$\dot{x}_6 = (x_2 \sin(x_4) + x_3 \cos(x_4)) / \cos(x_5) \quad (18)$$

where $\Gamma_i (i = 1, \dots, 8)$ is defined as:

$$\begin{aligned} \Gamma_1 &= \frac{I_{yy} - I_{zz}}{I_{xx}}, & \Gamma_2 &= \frac{I_{\text{rotor}}}{I_{xx}}, & \Gamma_3 &= \frac{1}{I_{xx}} \\ \Gamma_4 &= \frac{I_{zz} - I_{xx}}{I_{yy}}, & \Gamma_5 &= \frac{I_{\text{rotor}}}{I_{xx}}, & \Gamma_6 &= \frac{1}{I_{yy}} \\ \Gamma_7 &= \frac{I_{xx} - I_{yy}}{I_{zz}}, & \Gamma_8 &= \frac{1}{I_{zz}} \end{aligned} \quad (19)$$

Moreover, the measurement vector, obtained from the AHRS sensor is presented as follows:

$$\mathbf{z} = [p \ q \ r \ \phi \ \theta \ \psi]^T + v \quad (20)$$

where v is a Gaussian white noise. In the above equation, the superscripts T indicate the transpose notation.

3.5. Linear Model

The linear continuous-time model of the quadrotor platform about the equilibrium points ($\mathbf{x}_e \neq 0$ and $\mathbf{u}_e \neq 0$) is represented as:

$$\dot{\mathbf{x}}(t) = \mathbf{A} \mathbf{x}(t) + \mathbf{B} \mathbf{u}(t) + \mathbf{B}_d \mathbf{d}(t) \quad (21)$$

where $\dot{\mathbf{x}} = [\dot{x}_{\text{roll}} \ \dot{x}_{\text{pitch}} \ \dot{x}_{\text{yaw}}]$, defined as:

$$\mathbf{x}_{\text{roll}} = \begin{bmatrix} p \\ \phi \end{bmatrix}, \quad \mathbf{x}_{\text{pitch}} = \begin{bmatrix} q \\ \theta \end{bmatrix}, \quad \mathbf{x}_{\text{yaw}} = \begin{bmatrix} r \\ \psi \end{bmatrix} \quad (22)$$

where \mathbf{A} is the dynamic system matrix, denoted as:

$$\mathbf{A} = \begin{bmatrix} \mathbf{A}_{\text{roll}} & \mathbf{0} & \mathbf{0} \\ \mathbf{0} & \mathbf{A}_{\text{pitch}} & \mathbf{0} \\ \mathbf{0} & \mathbf{0} & \mathbf{A}_{\text{yaw}} \end{bmatrix} \quad (23)$$

Moreover, \mathbf{B} and \mathbf{B}_d are the input and disturbance matrices, respectively, and are defined as:

$$\mathbf{B} = \mathbf{B}_d = \begin{bmatrix} \mathbf{B}_{\text{roll}} & \mathbf{0} & \mathbf{0} \\ \mathbf{0} & \mathbf{B}_{\text{pitch}} & \mathbf{0} \\ \mathbf{0} & \mathbf{0} & \mathbf{B}_{\text{yaw}} \end{bmatrix} \quad (24)$$

In addition, the input matrices and state are shown as:

$$\mathbf{A}_{\text{roll}} = \mathbf{A}_{\text{pitch}} = \mathbf{A}_{\text{yaw}} = \begin{bmatrix} 0 & 0 \\ 1 & 0 \end{bmatrix} \quad (25)$$

$$\mathbf{B}_{\text{roll}} = \begin{bmatrix} \frac{1}{I_{xx}} \\ 0 \end{bmatrix}; \quad \mathbf{B}_{\text{pitch}} = \begin{bmatrix} \frac{1}{I_{yy}} \\ 0 \end{bmatrix}; \quad \mathbf{B}_{\text{yaw}} = \begin{bmatrix} \frac{1}{I_{zz}} \\ 0 \end{bmatrix} \quad (26)$$

3.6. Identification of the Platform Parameters

This section describes the utilization of the Nonlinear Least Squares (NLS) algorithm for estimating the model parameters (Γ) of the 3DoF experimental platform using experimental data. This technique is based on the Trust-Region Reflective Least Squares (TRRLS) method, which iteratively finds the values of the model parameters by minimizing a cost function, defined as follows:

$$\min_{\Gamma_i} (\| e(\Gamma_i) \|^2) = \min_{\Gamma_i} = \left(\sum_{j=1}^n (\mathbf{z}_j - \hat{\mathbf{z}}_j)(\mathbf{z}_j - \hat{\mathbf{z}}_j)^T \right) \quad (27)$$

where \mathbf{z} and $\hat{\mathbf{z}}$ are the experimental and simulated output signals, when the same input signals are applied ones. The structure of the proposed identification approach is illustrated in figure 4

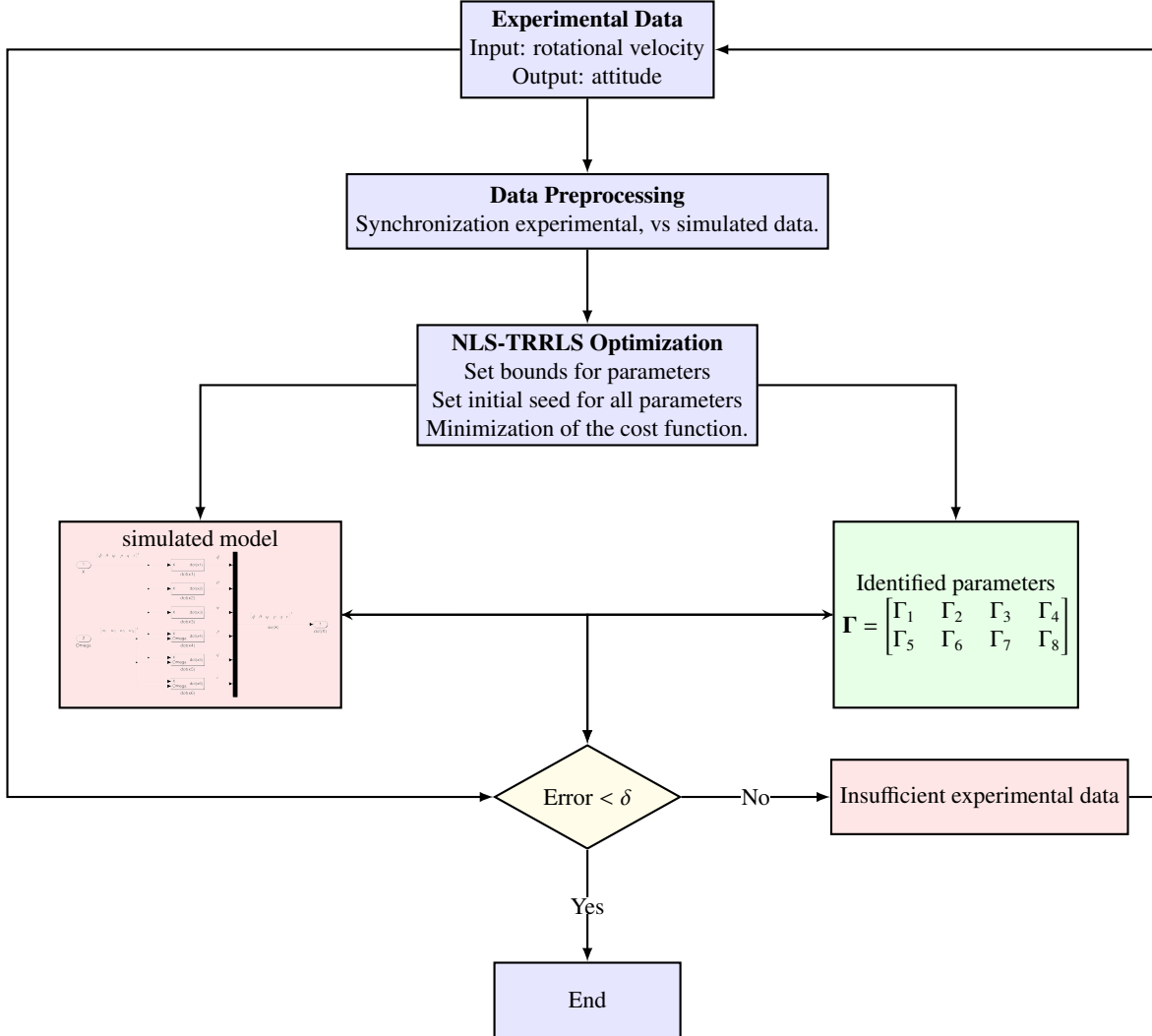


Figure 4: Structure of TRRLS identification approach.

4. Formulation of the LQDG Controller

Here, the LQR-DG controller is augmented with an integral action to eliminate steady-state errors. For this purpose, the augmented states of the quadrotor platform, which include states and their integrals, are selected. The design methodology of the LQR-DG controller is introduced. It generates optimal control signals for the three degrees of freedom platform.

4.1. Augmented State Space Development

To integrate the integrator into the control strategy architecture, the augmented state variables are defined below:

$$\mathbf{x}_{\mathbf{a}_i} = \begin{bmatrix} \mathbf{x}_i \\ \int \mathbf{x}_i \end{bmatrix} \quad (28)$$

The dynamics model of the quadrotor, as expressed by Eq. (21), is reformulated into an augmented state-space model that incorporates the roll (ϕ), pitch (θ), and yaw (ψ) angles. The augmented state-space model provides a

comprehensive description of the quadrotor's dynamic behavior, enabling the design of effective control strategies. The ensuing state-space model that integrates the augmented state variables is mathematically represented and defined in the following manner:

$$\dot{\mathbf{x}}_a(t) = \mathbf{A}_a \mathbf{x}_a(t) + \mathbf{B}_a \mathbf{u}(t) + \mathbf{B}_{d_a} \mathbf{d}(t) \quad (29)$$

\mathbf{B}_a and \mathbf{A}_a , which are expressed as below:

$$\mathbf{B}_a = \mathbf{B}_{d_a} = \begin{bmatrix} \mathbf{B} \\ \mathbf{0} \end{bmatrix} \quad (30)$$

$$\mathbf{A}_a = \begin{bmatrix} \mathbf{A} & \mathbf{0} \\ \mathbf{I} & \mathbf{0} \end{bmatrix} \quad (31)$$

In the aforementioned expression, the notation \mathbf{I} denotes the identity matrix.

4.2. LQR-DG Control Scheme with Integral Action

In line with the principles of differential game theory, the LQIR-DG controller is designed to be both robust and optimal. The LQIR-DG scheme involves selecting two fundamental players, one responsible for determining the control command and the other for generating the worst possible disturbance. To achieve the primary objective, the primary player minimizes the following cost function, while the other player must maximize it:

$$\min_u \max_d J(\mathbf{x}_{a_i}, d_i, u_i) = J(\mathbf{x}_{a_i}, u_i^*, d_i^*) = \min_d \max_u \int_0^{t_f} \left(\mathbf{x}_{a_i}^T \mathbf{Q}_i \mathbf{x}_{a_i} + u_i^T R u_i - d_i^T R_d d_i \right) dt \quad (32)$$

where \mathbf{Q}_i , R_d , and R are weight coefficients of the function. The final time is denoted by t_f . By solving the above problem, the control command is computed as follows [24]:

$$d_i(t) = \mathbf{K}_{d_i}(t) \mathbf{x}_{a_i}(t) \quad (33)$$

Moreover, the worst disturbance is obtained as:

$$u_i(t) = -\mathbf{K}_i(t) \mathbf{x}_{a_i}(t) \quad (34)$$

Here, \mathbf{K}_{d_i} and \mathbf{K}_i are gain values defined as follows:

$$\mathbf{K}_i = R^{-1} \mathbf{B}_{a_i}^T \mathbf{P}_{a_i}(t) \quad (35)$$

$$\mathbf{K}_{d_i} = R_d^{-1} \mathbf{B}_{a_{d_i}}^T \mathbf{P}_{a_{d_i}}(t) \quad (36)$$

where $\mathbf{P}_{a_i}(t)$ and $\mathbf{P}_{a_{d_i}}(t)$ satisfy

$$-\mathbf{A}_a^T \mathbf{P}_{a_{d_i}}(t) - \mathbf{Q}_i - \mathbf{P}_{a_{d_i}}(t) \mathbf{A}_a + \mathbf{P}_{a_{d_i}}(t) \mathbf{S}_{a_i}(t) \mathbf{P}_{a_i}(t) + \mathbf{P}_{a_{d_i}}(t) \mathbf{S}_{a_{d_i}}(t) \mathbf{P}_{a_{d_i}}(t) = \mathbf{0} \quad (37)$$

$$-\mathbf{A}_a^T \mathbf{P}_{a_i}(t) - \mathbf{Q}_i - \mathbf{P}_{a_i}(t) \mathbf{A}_a + \mathbf{P}_{a_i}(t) \mathbf{S}_{a_{d_i}}(t) \mathbf{P}_{a_{d_i}}(t) + \mathbf{P}_{a_i}(t) \mathbf{S}_{a_i}(t) \mathbf{P}_{a_i}(t) = \mathbf{0} \quad (38)$$

where

$$\mathbf{S}_{a_i} = \mathbf{B}_{a_i} R^{-1} \mathbf{B}_{a_i}^T, \quad \mathbf{S}_{a_{d_i}} = \mathbf{B}_{a_{d_i}} R_d^{-1} \mathbf{B}_{a_{d_i}}^T$$

5. Result and Discussion

Here, the simulation results of parameter identification and LQIDG-Controller for a quadrotor platform are presented. First, the quadrotor parameters are estimated based on the NLS method. Then, the performance of the LQDG controller structure is evaluated. The performance of the quadrotor LQIDG controller is presented in Tables 1 and 2.

Table 1: Quadrotor Parameters

Parameter	Value	Unit
d_{cg}	0.2	m
d	3.2×10^{-6}	N.m.sec ² /rad ²
b	3.13×10^{-5}	N.sec ² /rad ²
I_{xx}	0.02839	kg.m ²
I_{yy}	0.03066	kg.m ²
I_{zz}	0.0439	kg.m ²
I_{rotor}	4.4398×10^{-5}	kg.m ²
Ω_{mean}	3000	rpm

Table 2: LQIR-DG Controller Parameters

Channel	Weighting Matrix	Matrix Values
Roll	Q_{roll}	diag([0.02, 65.96, 83.04, 0.00])
Pitch	Q_{pitch}	diag([435.01, 262.60, 262.60, 0.00])
Yaw	Q_{yaw}	diag([4×10^{-4} , 0.00, 0.133, 0])
	R	1
	R_d	1.2764

5.1. Identification of the 3DoF quadrotor platform model

As described in section 3.4, the parameters of the quadrotor platform, denoted by $\Gamma_i (i = 1, \dots, 8)$, are identified using the NRS algorithm. The NLS-TRRLS algorithm is implemented in Matlab R2022b®. To increase the accuracy of parameter identification, three scenarios according to Table 3. In the first scenario, depicted in Figure 5, the quadrotor is rotated about only one axis (roll, pitch, or yaw axes) to identify the parameters Γ_3 , Γ_6 , and Γ_8 . In the second scenario, as illustrated in Figure 6, the parameters Γ_2 and Γ_5 are estimated by moving the experimental platform to freely rotate around its roll and pitch axes simultaneously. When the stopping condition of the NLS algorithm is met, the optimal values of the quadrotor parameters are computed and presented in Table 4. These results illustrate that the outputs of the simulation results for the quadrotor model are consistent with reality.

Table 3: Scenarios for Identification of Quadrotor Parameters.

Scenario	Description	Initial Condition (deg)			Rotational Velocity Commands			
		ϕ	θ	ψ	Ω_1	Ω_2	Ω_3	Ω_4
I	Roll free	38	-	-	2000	2000	2000	3400
	Pitch free	-	-15	-	3700	2000	2000	2000
	Yaw free	-	-	-75	2000	3300	2000	3300
II	Roll and Pitch free	8	-5	-	1700	3800	2400	1700
III	Roll, Pitch, and Yaw free	8	-3	-146	1700	3800	2400	1700

Table 4: True values of the quadrotor parameters.

Parameter	Value	Parameter	Value
Γ_1	-0.9622	Γ_5	3.6441×10^{-4}
Γ_2	-0.0154	Γ_6	7.5395×10^{-5}
Γ_3	5.4716×10^{-5}	Γ_7	0.1308
Γ_4	1.0457	Γ_8	4.3753×10^{-5}

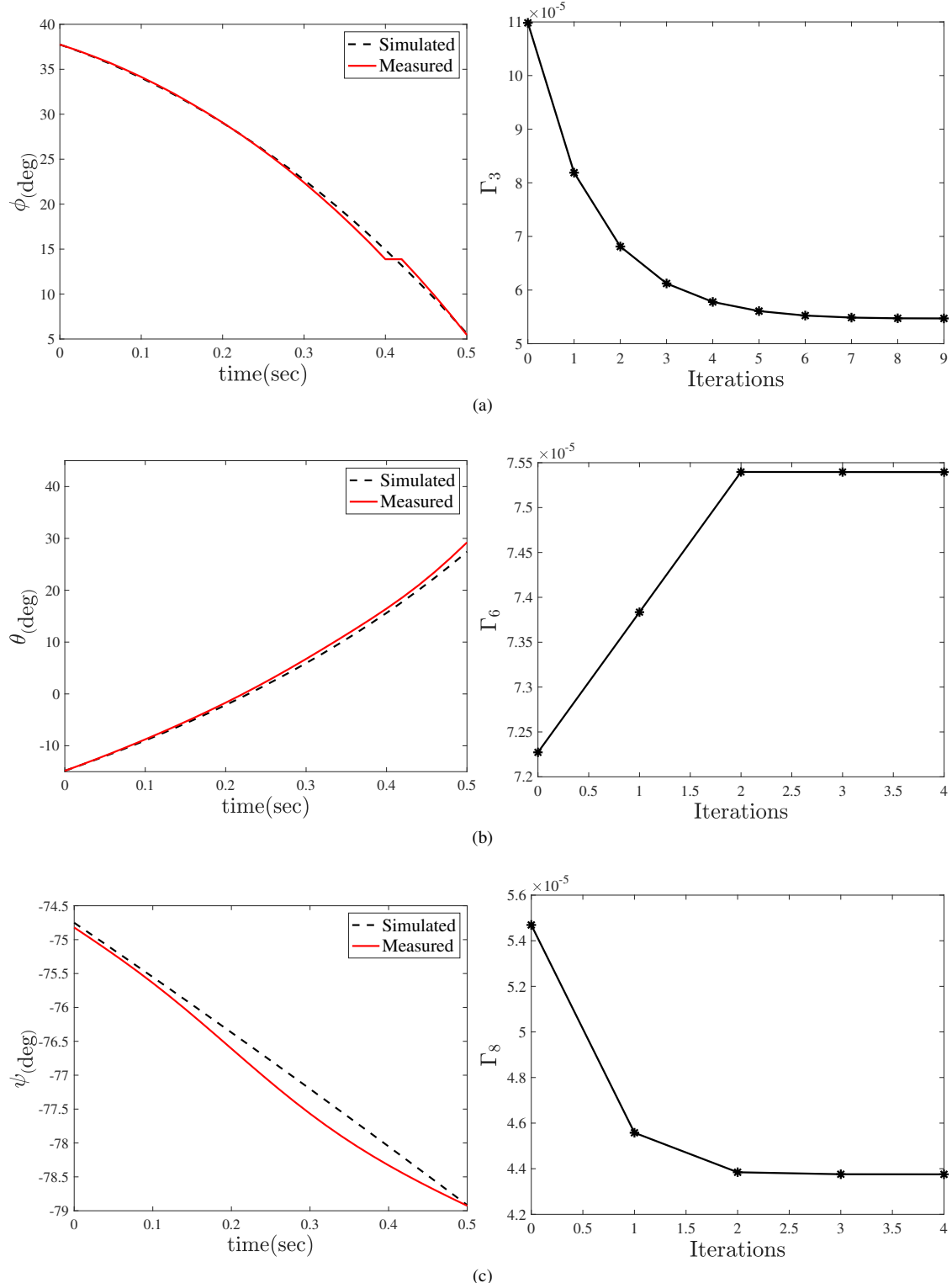


Figure 5: Identification process results when the quadrotor rotates about only one axis: (a) Identification of Γ_3 in free roll motion. (b) Identification of Γ_6 in free pitch motion. (c) Identification of Γ_8 in free yaw motion.

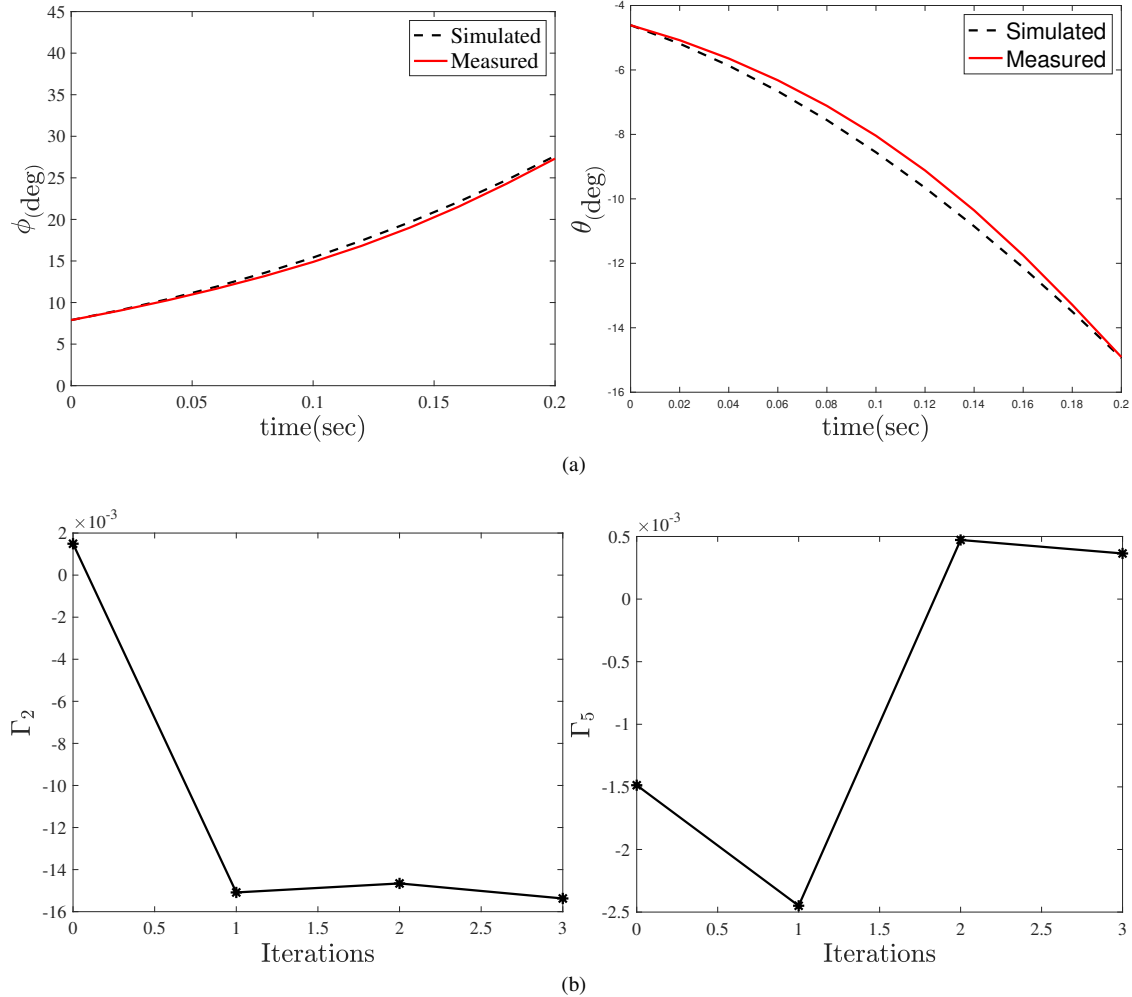


Figure 6: Identification process results when the quadrotor rotates about its roll and pitch axes: (a) Comparison of Simulation and experimental results. (b) Identification of Γ_2 and Γ_5 .

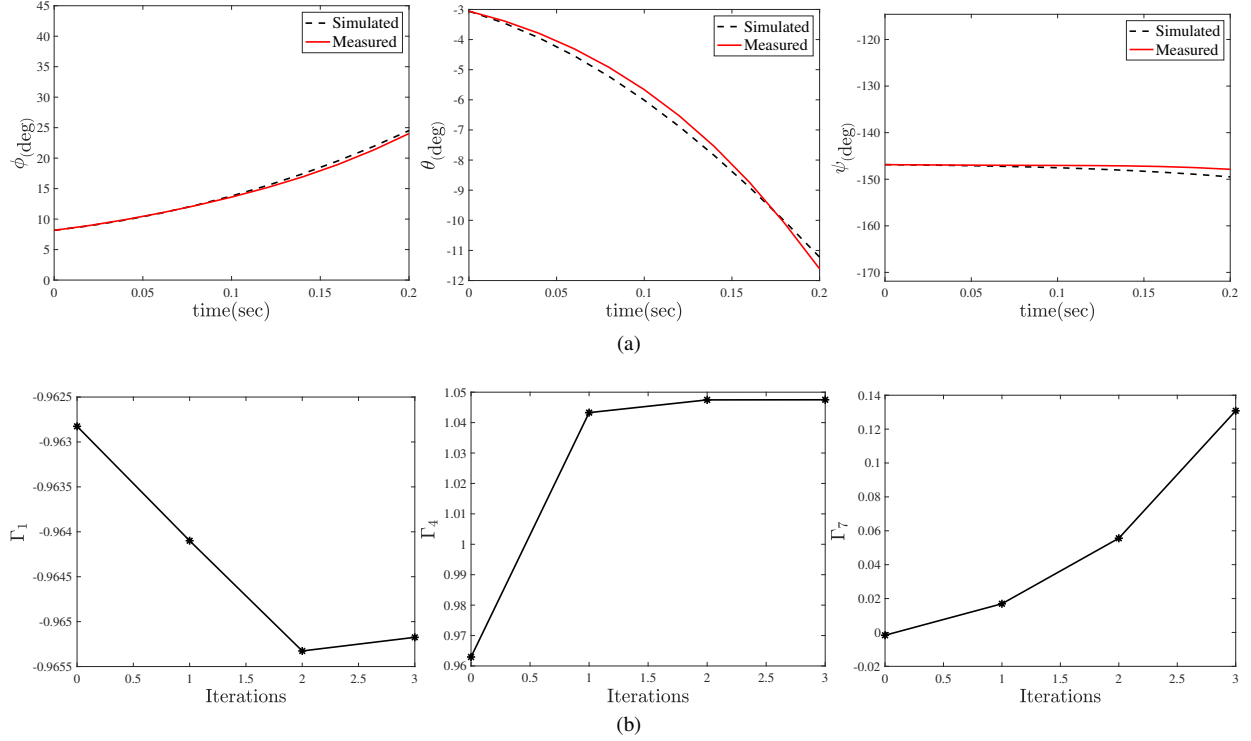


Figure 7: Identification process results when the quadrotor rotates about its roll, pitch, and yaw axes: (a) Comparison of Simulation and experimental results. (b) Identification of Γ_1 , Γ_4 and Γ_7 parameters.

5.2. Evaluation of LQIR-DG Performance

Here, the performance of the LQIR-DG controller algorithm is evaluated for regulation and tracking performance, disturbance rejection, and the impact of model uncertainty. Finally, the performance of the proposed controller is compared to the PID controller and variants of the LQR controller. The parameters of the PID controller are presented in Table 5.

Table 5: Parameters of PID Controller

Channel	K_p	K_i	K_d
Roll	2.0	0.5	1.0
Pitch	1.5	0.4	0.8
Yaw	3.0	0.6	1.2

5.2.1. Performance of the LQIR-DG Controller

Here, the results of the LQIR-DG controller method are presented for the control loops of the Euler angles of the experimental platform in Figures 8 and 9. The performance of the proposed controller is evaluated in Figure 8. Figure 8 (a) compares the desired and output signals, i.e., the Euler angles during regulation. Figure 8 (b) compares the desired square wave input with a frequency of 0.02 Hz and an amplitude of 20 degrees with the output signals in the two-degree-of-freedom coupling mode.

Moreover, Figures 9 (a) and (b) show the rotational velocity command of the quadrotor in the regulation and tracking problems, respectively. These results demonstrate that the roll, pitch, and yaw angles are accurately controlled by the proposed approach.

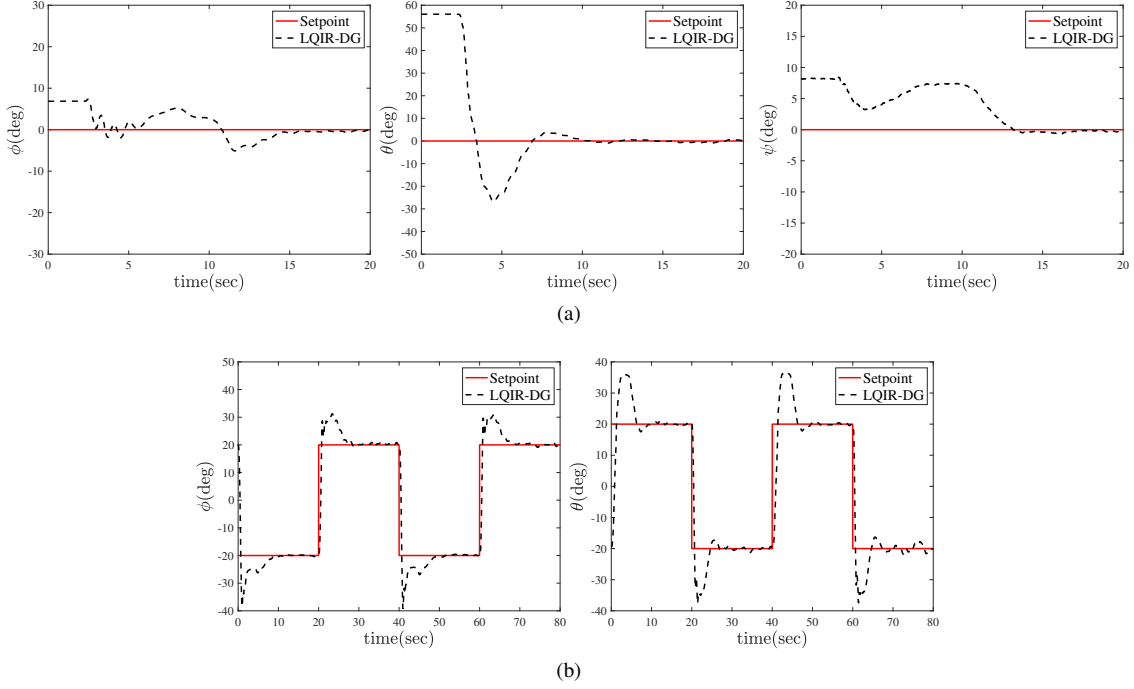


Figure 8: Comparison of Euler angles in (a) regulation (b) Tracking Conditions

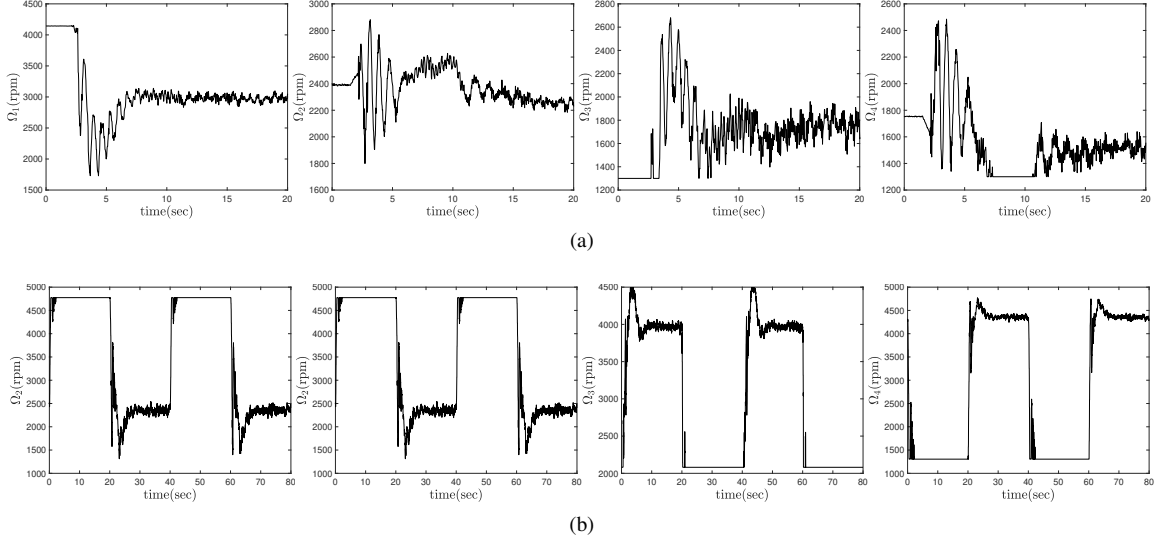


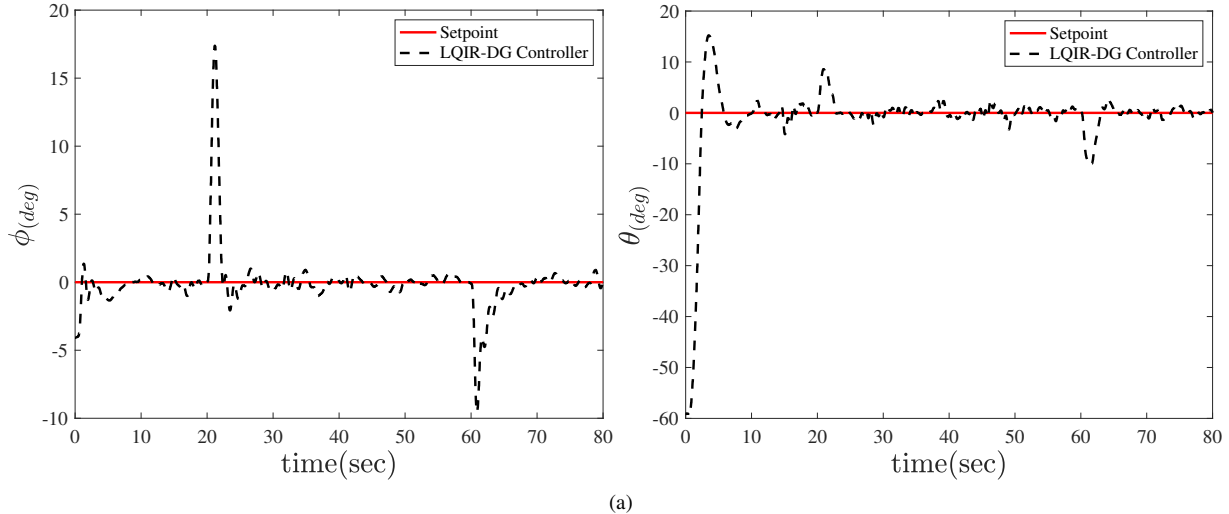
Figure 9: Temporal Evolution of Angular Velocity Commands for the LQIR-DG Controller

5.2.2. Performance of the LQIR-DG in Disturbance Rejection

The performance of the proposed controller in the input disturbance is shown in Figure 10. The input disturbance, $d\Omega_i$, is considered as a change in the command of the rotational velocity, modeled as:

$$d\Omega_1 = d\Omega_2 = -d\Omega_3 = -d\Omega_4 = \begin{cases} 500_{\text{rpm}} & 20 < t < 60 \\ 0 & \text{otherwise} \end{cases} \quad (39)$$

Figure 10 (a) illustrate the desired and the actual roll and pitch angles in the regulation problem. The results indicate that the LQIR-DG controller can stabilize the quadrotor platform when the input disturbance is present.



(a)

Figure 10: Comparison of the desired and actual roll and pitch angle in the presence of the input disturbance.

5.2.3. Investigating the Impact of Modeling Uncertainty

In this section, the performance of the LQIR-DG controller is investigated while considering uncertainty in the 3DoF experimental model. To achieve this, 50 and 100 grams were added to the roll and pitch axes, respectively, as shown in Figure 11. Figure 12 (a) compares the desired and the actual roll angle and Figure 12 (b) shows the desired and the actual pitch angle when the uncertainty of moments of inertia is presented. Moreover, Figure 12 (c) shows the rotational velocity command of the experimental platform in the presence of model uncertainty. The implementation results indicate that the LQIR-DG controller converges to the desired values in the presence of the modeling uncertainty.

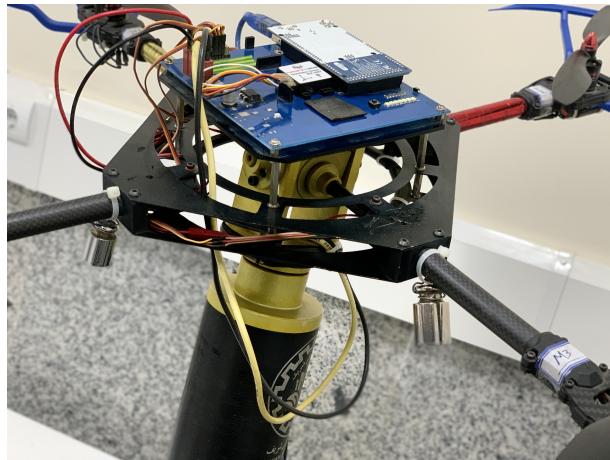


Figure 11: Quadrotor 3DoF Platform with Added Weight.

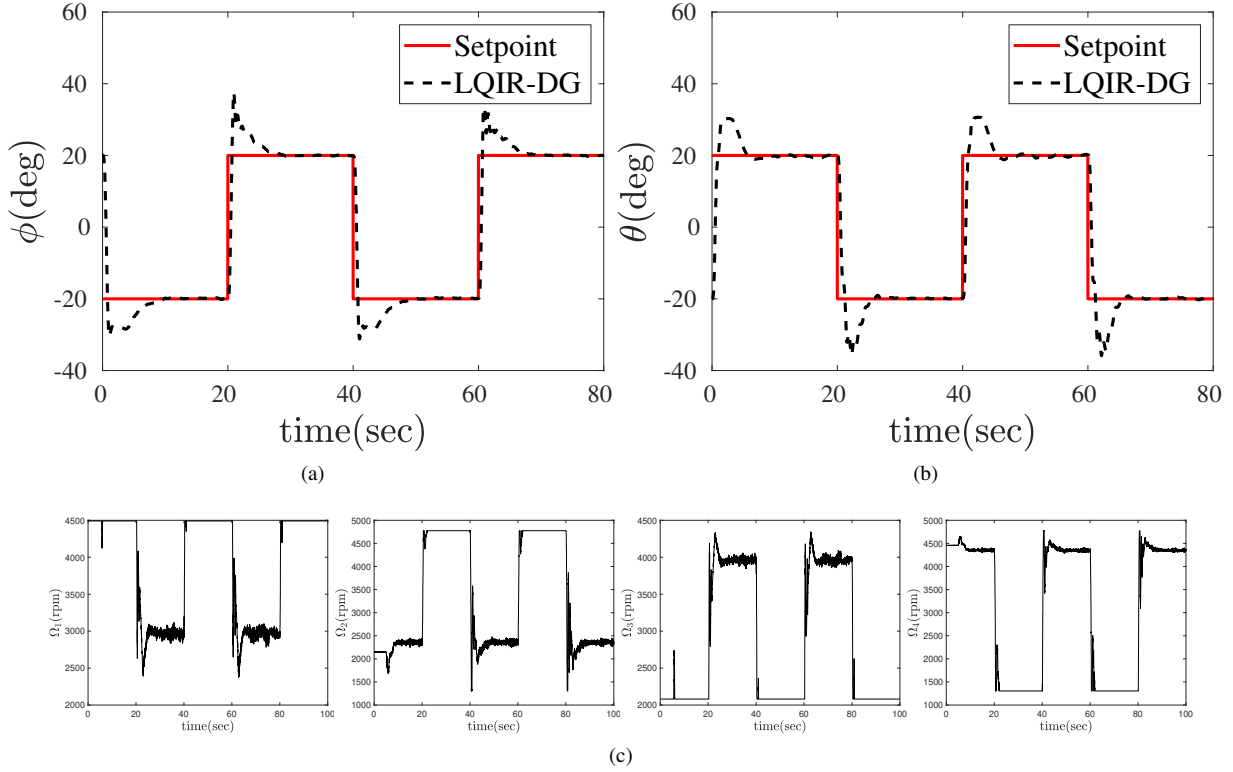


Figure 12: Comparison of the LQIR-DG controller when the uncertainty of moment of inertia is presented

5.2.4. Comparison with the Control Strategies

Here, the LQIR-DG controller performance is compared with the PID controller and variant of the LQR strategies such as the LQR and LQIR in Figure 13. Figure 13 compare the desired and the actual attitude of the quadrotor platform in the presence of these controllers. Moreover, the RSME of the controllers of all the controllers, i.e, boxplot, are compared in Figure 14. The median of RMSE is shown in the crossline in the boxplot.

These results indicate that the LQIR-DG controller is able to provide an excellent transient response and rapid convergence relative to other controllers for attitude control of the quadrotor experimental platform.

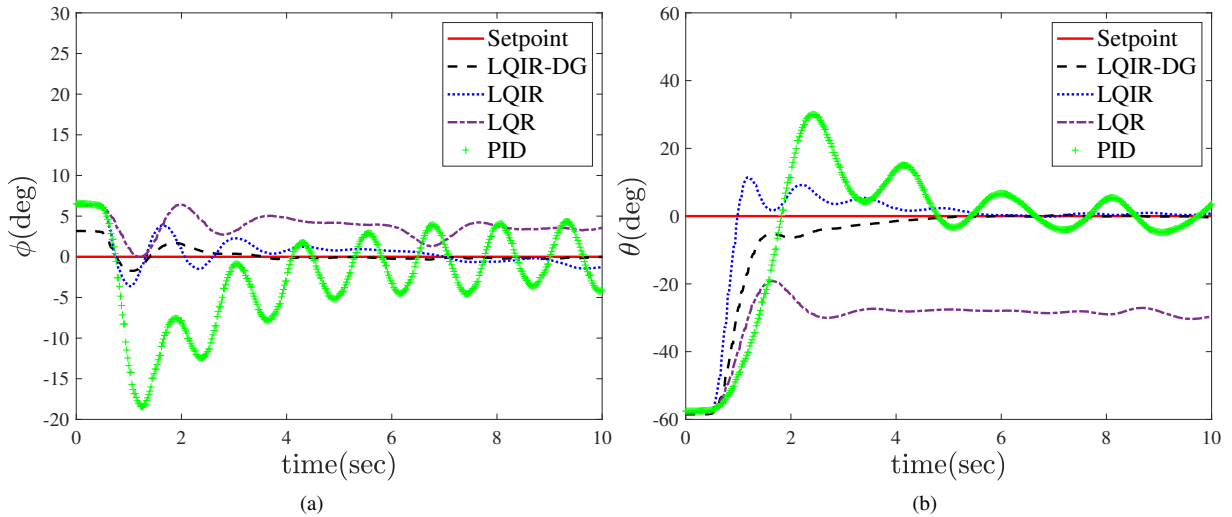


Figure 13: The implementation results of the LQIR-DG Control Strategy with added weight on the roll and pitch axes in the three-degree-of-freedom coupling mode. (a) Comparison of the desired roll angle with the actual roll angle, (b) Comparison of the desired pitch angle with the actual pitch angle.

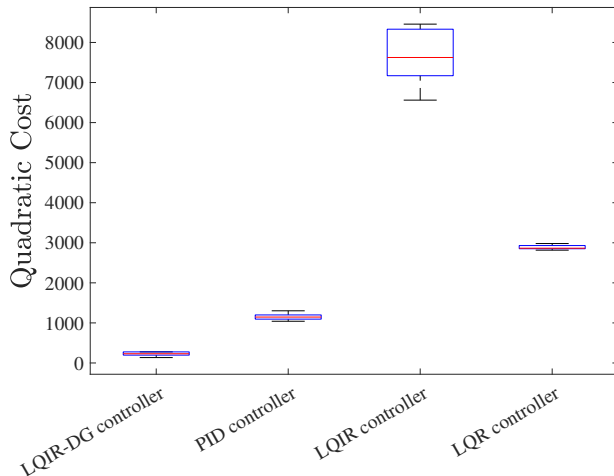


Figure 14: Comparative Analysis of the LQIR-DG Control Strategy versus LQR, LQIR, and PID Controllers using Quadratic Cost Function

6. Conclusion

In this paper, the LQIR-DG method, which is an optimal controller based on the game theory, was used in real-time for attitude control of an experimental platform for a quadrotor. To implement the proposed controller, an accurate dynamic model was considered for the quadrotor platform. Then, the model parameters were identified using the NSL method. For evaluation of the proposed method, the purpose of regulation and tracking problem was successfully performed. Moreover, the method's ability to reject the input disturbance and modelling error was investigated in the laboratory experiment. The implementation results illustrated the successful performance of the proposed method in attitude control for the quadratic platform.

References

- [1] M. F. Fathoni, S. Lee, Y. Kim, K.-I. Kim, K. H. Kim, Development of multi-quadrotor simulator based on real-time hypervisor systems, *Drones* 5 (3) (2021). doi:10.3390/drones5030059.
URL <https://www.mdpi.com/2504-446X/5/3/59>
- [2] H. Nobahari, A. Sharifi, A hybridization of extended kalman filter and ant colony optimization for state estimation of nonlinear systems, *Applied Soft Computing* 74 (10) 2018. doi:10.1016/j.asoc.2018.10.010.
- [3] H. Bolandi, M. Rezaei, R. Mohsenipour, H. Nemati, S. Smailzadeh, Attitude control of a quadrotor with optimized pid controller, *Intelligent Control and Automation* 04 (2013) 342–349. doi:10.4236/ica.2013.43040.
- [4] A. Abdul Salam, I. Ibraheem, Nonlinear pid controller design for a 6-dof uav quadrotor system, *Engineering Science and Technology, an International Journal* 22 (03 2019). doi:10.1016/j.jestch.2019.02.005.
- [5] Y. Bouzid, M. Zareb, H. Siguerdidjane, M. Guiatni, Boosting a Reference Model-Based Controller Using Active Disturbance Rejection Principle for 3D Trajectory Tracking of Quadrotors: Experimental Validation, *Journal of Intelligent and Robotic Systems* 100 (2) (2020) 597–614. doi:10.1007/s10846-020-01182-4.
URL <https://hal.univ-grenoble-alpes.fr/hal-02543214>
- [6] Z. Wang, D. Huang, T. Huang, N. Qin, Active disturbance rejection control for a quadrotor uav, in: 2020 IEEE 9th Data Driven Control and Learning Systems Conference (DDCLS), 2020, pp. 1–5. doi:10.1109/DDCLS49620.2020.9275226.
- [7] C. Nicol, C. Macnab, A. Ramirez-Serrano, Robust neural network control of a quadrotor helicopter, in: 2008 Canadian Conference on Electrical and Computer Engineering, 2008, pp. 001233–001238. doi:10.1109/CCECE.2008.4564736.
- [8] P. Ghiglino, J. L. Forshaw, V. J. Lappas, Online PID Self-Tuning using an Evolutionary Swarm Algorithm with Experimental Quadrotor Flight Results. arXiv:<https://arc.aiaa.org/doi/pdf/10.2514/6.2013-5098>
URL <https://arc.aiaa.org/doi/abs/10.2514/6.2013-5098>
- [9] L. V. Nguyen, M. D. Phung, Q. P. Ha, Iterative learning sliding mode control for uav trajectory tracking, *Electronics* 10 (20) (2021). doi:10.3390/electronics10202474.
URL <https://www.mdpi.com/2079-9292/10/20/2474>
- [10] C.-H. Pi, W.-Y. Ye, S. Cheng, Robust quadrotor control through reinforcement learning with disturbance compensation, *Applied Sciences* 11 (7) (2021). doi:10.3390/app11073257.
URL <https://www.mdpi.com/2076-3417/11/7/3257>
- [11] K. Liu, R. Wang, S. Dong, X. Wang, Adaptive fuzzy finite-time attitude controller design for quadrotor uav with external disturbances and uncertain dynamics, in: 2022 8th International Conference on Control, Automation and Robotics (ICCAR), 2022, pp. 363–368. doi:10.1109/ICCAR55106.2022.9782598.
- [12] K. Chara, A. Yassine, F. Srairi, K. Mokhtari, A robust synergetic controller for quadrotor obstacle avoidance using b閦ier curve versus b-spline trajectory generation, *Intelligent Service Robotics* 15 (03 2022). doi:10.1007/s11370-021-00408-0.
- [13] H. Wang, M. Chen, Sliding mode attitude control for a quadrotor micro unmanned aircraft vehicle using disturbance observer, in: Proceedings of 2014 IEEE Chinese Guidance, Navigation and Control Conference, 2014, pp. 568–573. doi:10.1109/CGNCC.2014.7007285.
- [14] A. Aboudonia, A. El-Badawy, R. Rashad, Disturbance observer-based feedback linearization control of an unmanned quadrotor helicopter, *Proceedings of the Institution of Mechanical Engineers Part I Journal of Systems and Control Engineering* 230 (07 2016). doi:10.1177/0959651816656951.
- [15] A. T. Azar, F. E. Serrano, A. Koubaa, N. A. Kamal, Backstepping h-infinity control of unmanned aerial vehicles with time varying disturbances, in: 2020 First International Conference of Smart Systems and Emerging Technologies (SMARTTECH), 2020, pp. 243–248. doi:10.1109/SMART-TECH49988.2020.00061.
- [16] A. Hamza, A. Mohamed, A. El-Badawy, Robust h-infinity control for a quadrotor uav, 2022. doi:10.2514/6.2022-2033.
- [17] W. Dean, B. Ranganathan, I. Penskiy, S. Bergbreiter, J. Humbert, Robust Gust Rejection on a Micro-air Vehicle Using Bio-inspired Sensing, 2017, pp. 351–362.
- [18] E. Barzani, K. Salahshoor, A. Khaki Sedigh, Attitude flight control system design of uav using lqr ltr multivariable control with noise and disturbance, in: 2015 3rd RSI International Conference on Robotics and Mechatronics (ICROM), 2015, pp. 188–193. doi:10.1109/ICRoM.2015.7367782.
- [19] Z. Shulong, A. Honglei, Z. Daibing, S. Lincheng, A new feedback linearization lqr control for attitude of quadrotor, in: 2014 13th International Conference on Control Automation Robotics and Vision (ICARCV), 2014, pp. 1593–1597. doi:10.1109/ICARCV.2014.7064553.
- [20] Z. Zwierzewicz, On the ship course-keeping control system design by using robust and adaptive control, in: 2014 19th International Conference on Methods and Models in Automation and Robotics (MMAR), 2014, pp. 189–194. doi:10.1109/MMAR.2014.6957349.
- [21] Y. Li, L. Guo, Towards a theory of stochastic adaptive differential games, in: 2011 50th IEEE Conference on Decision and Control and European Control Conference, 2011, pp. 5041–5046. doi:10.1109/CDC.2011.6160768.
- [22] S. Bouabdallah, R. Siegwart, Full control of a quadrotor, in: 2007 IEEE/RSJ International Conference on Intelligent Robots and Systems, 2007, pp. 153–158. doi:10.1109/IROS.2007.4399042.
- [23] S. Bouabdallah, Design and control of quadrotors with application to autonomous flying (01 2007). doi:10.5075/epfl-thesis-3727.
- [24] J. Engwerda, Linear quadratic games: An overview, Workingpaper, Macroeconomics, subsequently published in Advances in Dynamic Games and their Applications (book), 2009 Pagination: 32 (2006).